Stars Don't Eat Their Young Migrating Planets – Empirical Constraints On Planet Migration Halting Mechanisms

Peter Plavchan[1] and Christopher Bilinski[2]

ABSTRACT

The discovery of "hot Jupiters" very close to their parent stars confirmed that Jovian planets migrate inward via several potential mechanisms. We present empirical constraints on planet migration halting mechanisms. We compute model density functions of close-in exoplanets in the orbital semi-major axis – stellar mass plane to represent planet migration that is halted via several mechanisms, including the interior 1:2 resonance with the magnetospheric disk truncation radius, the interior 1:2 resonance with the dust sublimation radius, and tidal dissipation. We also compute model density functions for a planet halting distance that has no dependence on stellar mass to represent migration via external perturbers. We fit these model density functions to empirical distributions of known exoplanets and Kepler candidates that orbit interior to 0.1 AU. Migration halting at the interior 1:2 orbital resonance with the magnetospheric disk truncation radius provides the best fit to the empirical distributions that we test. We can rule out migration halting via tidal dissipation and migration halting at the interior 1:2 resonance with the dust disk sublimation radius. Our results favor a weak dependence of the halting distance with stellar mass, and is consistent with the decline in exoplanet frequency towards smaller orbital radii found in the Kepler candidates sample.

Subject headings: planetary systems: formation — planetary systems: protoplanetary disks

1. Introduction

Many "hot Jupiter" planets have been discovered to orbit very close to their central stars (e.g., Marcy & Butler 1998; Marcy et al. 1997; Borucki et al. 2011). It is well-established that these planets must form further out from their host stars, likely beyond the snow line, and either migrate embedded in a primordial disk or scatter inwards (e.g., Lin et al. 1996; Lubow & Ida 2010; Kozai 1962; Triaud et al. 2010). Observations of the Rossiter-McLaughlin effect to identify stellar

[1]NASA Exoplanet Science Institute, California Institute of Technology, M/C 100-22, 770 South Wilson Avenue, Pasadena, CA 91125

[2]University of Arizona

spin – planet orbit misalignment show that a significant fraction of "hot Jupiters" are aligned, and a significant fraction are also misaligned (Morton & Johnson 2011; Triaud et al. 2010). The mis-aligned planets are likely directed inwards via planet-planet scattering, the Kozai mechanism, secular chaos, or analogous mechanisms (e.g., Kozai 1962; Wu & Murray 2003; Naoz et al. 2011; Nagasawa & Ida 2011; Wu & Lithwick 2011).

For aligned close-in planets, planet migration embedded in a primordial disk is suspected to explain the observed planet location. Most disk migration models involve similar physical processes, but contain differences in the underlying assumptions about the structure and properties of the primordial disk and the planet (e.g., viscosity, density, scale height, temperature, dissipation time-scale, toroidal magnetic fields embedded in the disk, etc., Lin et al. 1996; Lubow & Ida 2010; Raymond et al. 2006; Menou & Goodman 2004; Tanaka et al. 2002; Terquem 2003). Current hypotheses often combine a few models together in an attempt to explain observed exoplanet mass and semi-major axis distributions. The justification cited is that conditions within the disk and the planet mass and density change over time, resulting in different models being applicable at different times in the planet migration process.

Type I migration assumes that the density structure of the disk is not affected by planets. Instead, turbulence determines the density structure of the disk. For this reason, this form of migration is most applicable to small mass planets. In the case of type II migration, a gap is formed between the disk and a high mass planet. This gap is the result of the tidal torques from the planet becoming stronger than the viscous torques of the disk. Initial theoretical models of Type I and Type II migration suggested a rapid planet migration rate that could result in planet destruction by dispersing the accreted material. Various mechanisms are thought to decrease the planet migration rate, including eccentric planet orbits and disk turbulence (Lubow & Ida 2010; Menou & Goodman 2004). In all cases, planet-disk migration must take place while the primordial disk of gas and dust is still present during the classical T Tauri phase, or first $\sim$5 Myr, of the host star's life (Silverstone et al. 2006; Currie et al. 2009).

Type II migration offers an effective mechanism to transport gas giants that must form beyond the snow line inward to their host star. However, it is not well-constrained how planet migration is halted once started, lest the planet be tidally disrupted by the host star. Possible braking mechanisms include – tidal excitation (the tidal "Q" factor) in the convective atmosphere of the host star (Arras et al. 2011; Matsumura et al. 2010; Lai 2011), trapping the exoplanet in the 1:2 interior orbital resonance with the magnetospheric truncation radius (Eisner et al. 2005), or trapping the planet in the 1:2 interior orbital resonance with the dust sublimation radius (e.g., Kuchner & Lecar 2002). For an approximately solar mass star, the gas disk truncation radius is comparable to the dust sublimation radius for a typical T-Tauri star magnetic field strength of $\sim$2 kGauss (Eisner et al. 2005), but that is not the case for lower and higher mass stars. For lower-(higher-)mass T Tauri stars, the dust sublimation radius can be interior (exterior) to the estimated magnetospheric truncation radius (§3).

In this work we investigate exoplanet distributions as a function of semi-major axis and host stellar mass as a test for migration halting mechanisms. The increasing number of exoplanet discoveries provides sufficiently large ensembles of close-in (e.g. <0.1 AU) exoplanets over a range of host stellar masses to discern which mechanism may be responsible for halting exoplanet migration. In §2, we outline our empirical samples. In §3, we present each migration halting mechanism model and its corresponding prediction for the exoplanet distribution density function. In §4, we present our methodology to evaluate the success of each migration halting model at reproducing empirical distributions, and in §5 we present the results of these statistical tests. In §6, we present our conclusions.

2. Empirical Samples

We make use of two empirical samples – confirmed exoplanets as of May 2011 (NASA Exoplanet Archive 2011; Wright et al. 2011), and the Kepler planetary candidates, also known as Kepler Objects of Interest (KOI, Borucki et al. 2011; Howard et al. 2011). We further sub-divide the Kepler candidates by estimated planet radius into three samples – all candidates, candidates with $R_{pl} > 5R_{\oplus}$, and candidates with $R_{pl} > 11R_{\oplus}$. These sub-divisions are chosen to approximate the super-Earth / Neptune, and Neptune / Jovian planet radii boundaries. Estimates of stellar mass are culled from the literature from the NASA Exoplanet Archive and exoplanets.org for the confirmed exoplanets. The Kepler Input Catalog stellar masses are utilized for the Kepler candidates (Brown et al. 2011). These four empirical samples are shown in Figure 1.

We exclude all exoplanets and candidates with orbital semi-major axes >0.1 AU to focus on close-in planets most likely to have undergone some form of migration in their orbital evolution, rather than forming in-situ at their present locations. We also constrain our samples to stellar masses of between 0.1 and 1.5 $M_{\odot}$. The upper limit of 1.5 $M_{\odot}$ is chosen to exclude planets around higher mass stars that can be evolved sub-giants (e.g., Johnson et al. 2011). The final exoplanet counts in each of our samples are: 126 for confirmed exoplanets, 649 for all Kepler candidates, 116 for Kepler candidates with $R_{pl} > 5R_{\oplus}$, and 39 for Kepler candidates with $R_{pl} > 11R_{\oplus}$.

Inherent in these samples are many survey biases and incompleteness. We discuss these briefly. The frequency of planets as a function of stellar mass is highly dependent on the survey sample selection criteria of ongoing searches. For example, the Kepler Input Catalog was selected to focus on FGK-type stars, with a paucity of M dwarfs (Borucki et al. 2011), and visible radial velocity searches initially focused on similar solar-mass stars (Marcy & Butler 1998). Additionally, there are likely real differences in the planet frequency as a function of planet mass and stellar mass that are not yet well constrained (e.g., Howard et al. 2011). Thus, in our analysis that follows we divide out the dependence of the planet density function by the frequency of exoplanets (within 0.1 AU) as a function of stellar mass. Further, we do not draw any conclusions about the planet frequency as a function of stellar mass.

The transit and radial velocity detection methods, responsible for the discovery of most close-in confirmed exoplanets, are highly biased towards the detection of short-period orbits. Additionally, at a fixed semi-major axis, planets around a lower-mass star will have a longer orbital period. This introduces bias towards a higher detection efficiency towards higher stellar masses at a fixed semi-major axis. However, most ground-based surveys are reasonably complete to within our semi-major axis cut of 0.1 AU, corresponding to an orbital period of $\sim$16 days for a solar-mass star. After more than two years of operation, Kepler is also (nearly) complete out to 0.1 AU, down to some nominal terrestrial planet size (Howard et al. 2011). Thus, we do not expect detection completeness as a function of semi-major axis to significantly impact our analysis.

Finally, for the known exoplanet sample, we do not apply any minimum constraint on planet mass (or planet mass limit in the case of radial velocity detected exoplanets). While terrestrial planets are more likely to have formed in-situ rather than migrated inward to their present locations, most known and confirmed exoplanets are Neptune-massed or larger, with a few Super-Earths. Thus, we do not expect the presence of a few low-mass planets in our sample to significantly impact our analysis, and we do not exclude them. Similarly, we do not correct for the false-positive rate in the Kepler exoplanet candidate list, which is though to be small (Howard et al. 2011; Borucki et al. 2011).

3. Migration Halting Models

For each migration halting mechanism model we present in this section, our goal is to generate a reasonably simple prediction for the density of exoplanets as a function of stellar mass and semi-major axis within 0.1 AU. We will present the model for each mechanism in turn, but first we outline commonalities in our methodology across models.

With the exception of the uniform random distribution model, our prescription involves first identifying a single 1:1 curve in the semi-major axis, stellar mass plane. The specification of these curves are outlined in subsections §3.1-3.4 for each particular model. We next convolve that curve with a Gaussian kernel in the log of the orbital semi-major axis to arrive at a predicted probability density function (PDF) to compare with an empirical distribution. The Gaussian width is a free parameter optimized for each model and empirical distribution combination we test. The use of a Gaussian kernel is an ad hoc step in our model generation, but its use is motivated by its simplicity and the observed scatter of exoplanet orbital semi-major axes.

Each model is next divided by the empirical frequency of exoplanets (within 0.1 AU) as a function of stellar-mass to correct for sample survey biases which are not relevant to our investigation herein (Figure 1). Finally, for computational simplicity, the PDF for each model is evaluated numerically on a 500 by 500 grid evenly spaced in stellar mass from 0.1 to 1.5 $M_{\odot}$ and in the log of the orbital semi-major axis in AU from log(a)=-2 to -1. The model density functions are summed over all pixels and the sum is normalized to 1.

3.1. The Interior 1:2 Orbital Resonance with the Accretion Disk Truncation at the Magnetospheric Radius

The magnetosphere of a T Tauri star has long been thought to truncate the inner accreting primordial gas disk (e.g., Chiang & Goldreich 1997; Meyer et al 1997), and recent interferometric observations of young stars confirm these inner holes exist (Eisner et al. 2005). A Jovian exoplanet undergoing Type II migration in a primordial disk could halt after it enters into this inner clearing, as has been proposed (Eisner et al. 2005; Kuchner & Lecar 2002; Lin et al. 1996). In this scenario, a migrating Jovian exoplanet interacts with a protoplanetary disk at Lindblad resonances, transferring angular momentum via torques to the disk as the planet migrates inward. When the 2:1 Lindblad resonance site enters the evacuated portion of the disk, the planet can no longer transfer angular momentum to the disk and the migration is hypothesized to halt. The exoplanet continues to orbit the host star at a period equal to one-half of the Keplerian orbital period of the magnetospheric gas disk truncation radius. A related but distinct halting mechanism is proposed for smaller planets undergoing Type I migration in Tsang (2011).

The magnetospheric radius can be approximated by (Eisner et al. 2005; Konigl 1991):

$$R_{mag} = 2.27 R_1 \left[\frac{(B_0/1\mathrm{kG})^4 (R_*/R_\odot)^5}{(M_*/M_\odot)(\dot{M}/(10^{-7} M_\odot \mathrm{yr}^{-1}))^2} \right]^{1/7} \tag{1}$$

where B_0 is the stellar magnetic field strength. A field strength of 2 kG is typical for T Tauri stars (Johns-Krull et al. 2003), and is a free parameter in our model density function. $\dot{M}$ is the stellar accretion rate in units of $M_\odot \mathrm{yr}^{-1}$, which can vary by several orders of magnitude for young stars. Muzerolle et al. (2003) derives an approximate power law relationship between stellar mass and accretion rate of $\dot{M} \propto M^2$. We estimate a proportionality constant of $10^{-8.5} M_\odot \mathrm{yr}^{-1}$ that yields appropriate accretion rates for solar type stars as inferred from Muzerolle et al. (2003, Figure 8). For a 2 kG field, the magnetospheric truncation radius is thus approximately given by:

$$R_{mag} = 9.05 R_\odot \left(\frac{R_*}{R_\odot} \right)^{12/7} \left(\frac{M_\odot}{M_*} \right)^{5/7} \approx 9 R_* \tag{2}$$

The 1:2 interior orbital resonance with this inferred magnetospheric radius is thus located at $\sim$6R$_*$ for a 2 kG stellar magnetic field, and our full migration halting semi-major axis location, a, is given by:

$$a = 9.05 R_\odot \left(\frac{B_0}{2\,\mathrm{kG}} \right)^{4/7} \left(\frac{R_*}{R_\odot} \right)^{\frac{12}{7}} * \left(\frac{M_\odot}{M_*} \right)^{\frac{5}{7}} * \frac{1}{2}^{2/3} \tag{3}$$

Finally, to arrive at our model analytic curve, we assume $\log g = 4$ as is typical for T Tauri stars that are still contracting onto the main sequence (Greene & Lada 1996). With these assumptions, we can express this migration halting radius as a function of only B_0 and M_*. The Gaussian

kernel that we use to generate the model exoplanet density function from the analytic curve in Equation 3 can be interpreted to represent the degenerate range in magnetic field strengths, stellar accretion rates, and/or stellar surface gravity about the assumed values. For example, the range of observed T Tauri accretion rates ($\sim$100, Muzerolle et al. 2003) would correspond to a range for a in Equation 1 of a factor of $\sim$2. Additionally, the pre-main sequence contraction times imply that the median magnetic field strength should vary as a function of stellar mass due to the range of different evolutionary states at a fixed proto-stellar age. Finally, exoplanet Type II migration may also preferentially take place at different stellar ages as a function of stellar mass (Lubow & Ida 2010; Lin et al. 1996). In our analysis that follows, however, we assume that we are only varying the magnetic field strength, and we keep the median magnetic field strength constant as a function of stellar mass. At this time, we do not overcomplicate our model to account for these various degenerate factors, given the success of this particular model (§5).

3.2. The Interior 1:2 Orbital Resonance with the Dust Disk Sublimation Radius

The truncation of the dust disk at the dust sublimation radius is also proposed as a mechanism to halt the inward migration of Jovian planets for solar type stars (Kuchner & Lecar 2002; Lin et al. 1996). This scenario for migration halting is identical to that for the magnetospheric truncation model in §3.1, except the planet is hypothesized to halt instead at the interior 1:2 orbital resonances with the dust disk sublimation radius. While the primordial (gas and dust) disk for a typical T Tauri star is thought to dissipate by a stellar age of $\sim$5 Myr, a debris dust disk from the collision of planetesimals can persist for much longer. For a solar-mass star, the dust sublimation radius is approximately equal to the expected magnetospheric gas disk truncation radius, and thus solar-type stars alone are a poor discriminator of migration halting mechanisms. However, the dust sublimation radius has a significantly different dependence on stellar mass when compared to the magnetospheric gas disk truncation radius.

The dust sublimation radius is given approximately by the expression (Jura et al. 1998):

$$R_{subl} = \frac{1}{2} R_* \left(\frac{T_*}{1500} \right)^2 \tag{4}$$

where T_* is the effective temperature of the host star in Kelvin, R_* is the radius of the host star, and we have assumed a dust sublimation temperature of 1500 K. Equation 4 assumes that the dust can be approximated by a blackbody in local thermal equilibrium, and that the dust is optically thin to the incident stellar radiation. Assuming to the contrary for both factors would decrease the dust sublimation radius. Viscous heating in a primordial disk can increase the dust sublimations radius, and more sophisticated treatments yield a stronger dependence of the sublimation radius on the stellar temperature (Robitaille et al. 2006, 2007; D'Alessio et al. 2006). In our analysis we retain the approximation in Equation 3 for simplicity, but also because of the lack of success for

this particular model (§5).

We adopt a temperature–radius relation using a Siess et al. (2000) 10 Myr isochrone to express the migration halting radius, a, as a function of only the stellar radius, e.g.:

$$a = \frac{1}{2}^{5/3} \left(\frac{T_{*\mathrm{Siess}}(R_*)}{1500} \right)^2 R_* \tag{5}$$

where the extra factor of $1/2^{\frac{2}{3}}$ comes from Kepler's laws and the 1:2 interior resonance location with respect to the dust sublimation radius in Equation 4. Our results are not significantly altered if we instead use a 10 Myr isochrone from Baraffe et al. (1998).

We adopt the age isochrone of 10 Myr with the assumption that the exoplanet migration must take place early in a star's evolution. An older stellar age will decrease the modeled migration halting radius in Equation 5, since the star will continue to contract onto the main sequence. Finally, to arrive at our model analytic curve, we again assume $\log g = 4$ in order to express this migration halting radius as a function of only M_*. The Gaussian kernel that we use to generate the model exoplanet density function from Equation 5 can be interpreted to represent a degenerate range in stellar surface gravity and/or dust sublimation temperatures about the assumed values.

Since the stellar effective temperature varies little over the main sequence lifetime of the host star, we can also estimate the distance a in Equation 5 for older main sequence stars. For main sequence M dwarfs, we note that the semi-major axis in Equation 5 for this orbital resonance is less than $\sim$2.2 R_*. This orbital separation falls within the estimated Roche radius of $\sim$2.4 R_* (§3.3), and a planet at this distance would likely be tidally disrupted. We conclude that no migrating Jovian planets survive around M dwarfs if the orbital resonance with the dust sublimation radius is responsible for braking Jovian planet migration, and the migration takes place after the M dwarfs have reached the main sequence. The expected exoplanet detection frequency for this scenario is zero for M dwarfs. While this is an interesting potential mechanism to explain the observed lack of M dwarf hot Jupiters relative to solar-mass stars (Endl et al. 2006; Plavchan et al. 2008), we do not find this scenario likely given our results in §5.

3.3. Tidal Excitation Radius

Next, we consider the hypothesis that the tidal excitation of the convective atmosphere of the parent star can result in an angular momentum transfer that halts exoplanet migration. This halting mechanism is analogous to the tidal circularization of the orbits of close-in exoplanets. In order for this mechanism to operate effectively, the exoplanet must get close to the tidal disruption radius of the star (Arras et al. 2011). Thus, under this mechanism we assume that the exoplanet halts at just outside the Roche Radius a given by:

$$a = R_*(2\rho_*/\rho_{pl})^{\frac{1}{3}} \quad (6)$$

where ρ_* and ρ_{pl} are the mean stellar and exoplanet densities respectively. To arrive at our model analytic curve, we assume again that $\log g = 4$ to estimate the stellar density. We also assume an exoplanet density equal to 0.25 g/cm^3, which is less than the density for Jupiter of 1.3 g/cm^3. We adopt this lower density, comparable to the density of HD 209458b of 0.37 g/cm^3 (NASA Exoplanet Archive 2011), since a young proto-planet would likely be self-luminous and still contracting. A higher planet density would decrease the migration halting radius in Equation 6. The estimated halting radius is a few times smaller than the magnetospheric disk truncation halting radius, which is sufficient to discern between the two halting mechanisms. Finally, the Gaussian kernel used to generate the model exoplanet density function from Equation 6 can be interpreted to represent a degenerate range of exoplanet and/or stellar densities about these assumed typical values.

3.4. Planet-Planet Scattering and Kozai Mechanism

Planet-planet scattering, resonance-driven migration of multiple exoplanets, secular chaos, and the Kozai mechanism offer additional mechanisms to migrate a Jovian exoplanet inwards towards its host star (Kozai 1962; Naoz et al. 2011; Nagasawa & Ida 2011; Wu & Lithwick 2011; Wu & Murray 2003). Some of these mechanisms are thought to be required to explain the known fraction of spin-orbit misaligned close-in exoplanets (Morton & Johnson 2011; Triaud et al. 2010). The association of the observed spin-orbit misalignment with the Kozai and similar migration mechanisms relies on the assumption that the stellar spin axis is aligned with the primordial disk rotation axis. This star-disk alignment is intuitively expected from the process of star formation. Exoplanets that undergo migration embedded in an aligned disk should yield an exoplanet orbit that remains aligned with the stellar spin axis, and therefore the observed misaligned exoplanets cannot be explained via disk migration. However, the observed spin-orbit misalignment could be produced by an embedded exoplanet migrating in a misaligned primordial disk. Recent observations of debris disks show no significant misalignment between the disk and star, in support of the need for a Kozai or similar migration mechanism (Watson et al. 2011). However, there are other proposed alternatives to explain spin-orbit misalignment, such as external perturbers after migration is completed as predicted for the multi-planet 55 Cnc system (Kaib et al. 2011), and disk warping from late-stage gas accretion from the accretion envelop (Thies et al. 2011).

The Kozai and similar migration mechanisms initially depend on (chaotic) dynamical interactions between exoplanets and/or external perturbers, as opposed to the mass of the host star. The final position of a planet that migrates via the Kozai mechanism is thought to be determined by the tidal circularization time-scale. Tidal circularization is predicted to be more effective for low-mass stars with deeper convective atmospheres (Kozai 1962; Wu & Murray 2003; Arras et al. 2011), and consequently one may predict closer-in orbits around higher mass stars. However, the

tidal circularization time-scale must be convolved with the Kozai migration rate to predict the final exoplanet distribution in semi-major axis. Thus the final exoplanet distribution remains highly dependent on the dynamical interactions with the external perturber as opposed to the mass of the host star. Thus, we generate two additional models for the close-in exoplanet density function to represent inward exoplanet migration under the Kozai and similar mechanisms. The first assumes a stellar-mass independent semi-major axis distribution about a singular value, A, and the second is a uniform random distribution. The first model is again convolved with a Gaussian kernel in the log of the semi-major axis, and the position of the Gaussian center $A(= \log a)$ as well as the width σ are free parameters in the model. The uniform random model can be thought of as a control test, since it makes no prediction about the distribution of exoplanets in the log of the semi-major axis – stellar mass plane. This distribution is not the same as a uniform random distribution in the semi-major axis – stellar mass plane, which would correspond to an exponential distribution in the log of the semi-major axis – stellar mass plane.

4. Methodology for Evaluating Model Success

We use a variety of different free parameters for our models as described in §3. To evaluate which migration braking mechanism is best at reproducing the different empirical distributions, and to determine optimal parameters, we use two approaches. We discuss each in turn.

4.1. Bayesian Evaluation

We use a Bayesian analysis to estimate the posterior probability $P\left(H_i|\, D\right)$ of obtaining a given empirical data set $D = \{D_j\}$ for a particular migration braking model hypothesis H_i. Explicitly, we re-state Bayes' Theorem:

$$P\left(H_i|\, D\right) = \frac{P\left(H_i\right) P\left(D\,|H_i\right)}{P(D)} \tag{7}$$

To optimize the parameter selection for a given empirical data set D and model H_i, we maximize the posterior probability $P\left(H_i|\, D\right)$ for the same model over a range of its free parameters. A second Bayesian test is then used to compare the models against one another after the best fit parameters have been selected.

Following the Bayesian technique, we obtain the likelihoods $P\left(D\,|H_i\right)$ by multiplying together the individial probability density functions $PDF_{H_i}(D_j)$ to calculate the probability of obtaining a single D_j:

$$P\left(D\left|H_i\right.\right) = \prod_j PDF_{H_i}(D_j) \tag{8}$$

where D_j is the semi-major axis and stellar host mass value pair for an individual exoplanet. We use the probability densities as described in §3 to estimate each individual $PDF_{H_i}(D_j)$, linearly interpolating from the 500x500 model grid.

For the prior terms, $P\left(H_i\right)$, we make three assumptions, with the first two applying to the Bayesian analysis for the optimal parameter selection. First, we assume a uniform prior for the B_0 and A parameters in the magnetospheric disk truncation and stellar mass independent models respectively (e.g., $\frac{\partial(P(H_i))}{\partial B_0} = \frac{\partial(P(H_i))}{\partial A} = 0$), since these parameters can vary directly with the predicted semimajor axis. Second, we use an uninformed Jeffrey's prior of $\frac{1}{\sigma}$ (e.g. $P(H_i) \propto \frac{1}{\sigma_i}$) for the Gaussian width σ parameter present in four of the models. To normalize a given model prior such that $\sum_i P\left(H_i\right) = 1$ in the discrete limit, we have that $P(H_i) = \frac{C}{\sigma_i}$ where $C = 1/\sum_i \frac{1}{\sigma_i}$, and $\{\sigma_i\}$ are the discrete set of widths evaluated in our analysis. Third, when we compare the different models against one another after parameter optimization, we re-set the prior terms equal to a constant - ie, we assign equal weight to the different model hypotheses to compare the relative success of each model given the set of optimal parameters. We also compute the posterior probabilities for models while taking into account all parameter combinations tested and corresponding likelihoods, as opposed to comparing only the models with the best fit parameters. This results in unequal weighting in evaluating to the "success" of a given model, and is dependent on the range of parameters explored for a given model. Thus, we only present the equal prior weighting results herein. Our relative ordering of preferred models are not altered with either analysis approach, and the equal prior weighting approach yields the more conservative relative posterior probabilities when comparing models.

The last term in Bayes' theorem needed to compute the posterior probabilities is the marginal probability, $P(D)$. However, we can rewrite this term as

$$P(D) = \sum_i P\left(D\left|H_i\right.\right) P\left(H_i\right), \tag{9}$$

where we sum over all hypotheses, i. We do not have an exhaustive list of models. Additionally, we include an arbitrary normalization N in our analysis to avoid the double data type machine precision limit. Thus, we do not obtain absolute posterior probabilities, and we can end up with relative posterior probabilities greater than 1. Nevertheless, we know that the value of $N/P(D)$ is the same in all of our computations, so we can ignore it and compute accurate relative posterior probabilities when we are comparing parameters or models. In other words, the quantity of interest is:

$$\frac{P\left(H_1\right| D)}{P\left(H_2\right| D)} = \frac{N\, P\left(H_1\right) P\left(D\left|H_1\right.\right)}{P(D)} \times \frac{P(D)}{N\, P\left(H_2\right) P\left(D\left|H_2\right.\right)} = \frac{P\left(H_1\right) P\left(D\left|H_1\right.\right)}{P\left(H_2\right) P\left(D\left|H_2\right.\right)} \tag{10}$$

4.2. Chi-Squared Tests

In order to test the predicted exoplanet density function against the empirical planet distributions using the chi-squared test, we first generate a density function for the empirical planet distributions. This was not necessary for the Bayesian analysis, which directly tested the empirical distribution of exoplanets against the model density function.

The density function is calculated for each data set using a kernel density estimation method analogous to that in (Wasserman 2005). Each exoplanet (or candidate) in the stellar mass – log orbital semi-major axis plane is convolved with a Gaussian kernel. The width of the Gaussian kernel is set to 0.165 in stellar mass in solar units, and 0.165 in the log of the orbital semi-major axis in AU. These particular widths are chosen from the median separation between exoplanets in the confirmed exoplanet empirical distribution, which were identified to be 0.167 log AU in the log of the semi-major axis and 0.164 $M_\odot$ in the stellar mass. The same kernel width is used for all four empirical data sets. The kernels are summed to produce the empirical density functions shown in Figure 1. As was done for the migration halting models, each empirical distribution is evaluated numerically on a 500 by 500 grid evenly spaced in stellar mass from 0.1 to 1.5 $M_\odot$ and in the log of the orbital semi-major axis in AU from log(a)=-2 to -1. This enables a direct subtraction of the model probability density function from the empirical density function to calculate the reduced χ^2 statistic.

5. Results

Our results are presented in Tables 1 through 3. Table 1 presents the optimal parameters for a given model and empirical data set from our Bayesian analysis. Table 2 summarizes the relative posterior probabilities for a given model and optimal parameters. Table 3 summarizes the corresponding reduced χ^2 values. Figures 2-10 show our best fit model density functions and residuals as a function of the data set (Figs 2-5) and model (Fig 6-10).

For every data set, migration halting at the interior resonance with the magnetospheric disk truncation radius provides the best fit to the data using both the Bayesian and χ^2 analysis. The model representing Kozai and similar mechanisms with a stellar-mass independent distribution about a constant semi-major axis is the second best model. The remaining models of tidal dissipation, halting interior to the dust sublimation radius, and a uniform random distribution in the log of the semi-major axis are strongly disfavored by the Bayesian analysis.

A "χ by eye" analysis of the figures agrees with our statistical results, showing that the magnetospheric disk truncation radius model and stellar mass independent model have the smallest residuals. The difference between these two best models is not clear "by eye," but the chi-squared test demonstrates a slight preference for the magnetospheric disk truncation radius halting model for all data sets. Furthermore, our Bayesian analysis does not rely on a Gaussian kernel estimate

of the empirical density function, which is used in the chi-squared analysis (§4.2) and is shown in Figures 2-10. Our Bayesian analysis computes the relative posterior probability directly from the empirical distribution of exoplanets, and demonstrates that the magnetospheric disk truncation radius halting model is consistently preferred to the stellar-mass independent halting model by factors of 1.8–30 for a given data set.

The best fit magnetospheric disk truncation model magnetic field strengths range from 1.15–2.9 kGauss for each of our data sets, consistent with observed T Tauri magnetic field strengths given our assumptions about the mass accretion rates in §3.1 (Johns-Krull et al. 2003; Eisner et al. 2005). We do not draw any conclusions about the best fit values for the Gaussian kernel width σ in the log of the semi-major axis, except to note that it provides a reasonable fit to the data. We do not attempt to explain the additional sub-structure in the estimated empirical probability density function that can be seen in Figure 1 for all data sets, but note that such sub-structure could point to multiple migration-halting mechanisms operating. Finally, for the best fit stellar-mass independent model, the preferred mean value of $a = 10^A$ ranges from 0.044 to 0.079 AU as expected for the close-in exoplanets.

6. Conclusions

We use the empirical distribution of confirmed exoplanets and Kepler planet candidates in the host stellar mass – exoplanet orbital semi-major axis plane as a diagnostic for migration halting mechanisms. Migration braking at the interior 1:2 orbital resonance with the magnetospheric disk truncation radius provides the best fit in all tests. For exoplanet orbits that are aligned with the stellar spin, this mechanism is likely responsible for halting Type II migration. We can rule out migration halting at the tidal excitation radius and the 1:2 interior resonance with the dust sublimation radius as viable mechanisms for the majority of observed close-in exoplanets. Our results favor a weak dependence of the halting distance with stellar mass as opposed to no dependence or a strong dependence.

Howard et al. (2011) report the decreasing planet frequency towards smaller orbital separations within $\sim$0.04 AU. Our analysis confirms that the observed dearth of Kepler exoplanet candidates at these small orbital radii, and this distribution does not favor migration halting via tidal excitation of the host star. The magnetospheric disk truncation model fit to the empirical data is best for the $R_{pl} > 11R_\oplus$ and $R_{pl} > 5R_\oplus$ Kepler exoplanet candidate sub-samples, and is worst for the unconstrained Kepler candidate data set. We interpret this to mean that the smallest Kepler exoplanet candidates likely do not migrate, and instead form in situ. This result is consistent with core accretion theory (Lin et al. 1996), and this transition occurs below a planet radius of $\sim 5R_\oplus$, corresponding to the transition between terrestrial and Neptune-like exoplanets.

For the magnetospheric disk truncation radius migration braking model, future efforts can replace the Gaussian kernel in the log of the semi-major axis with an incorporation of empirical

distributions for magnetic field strength, accretion rate, and surface gravities as a function of stellar mass to perhaps better model the observed sub-structure in the empirical distribution of exoplanets.

This research has made use of the NASA Exoplanet Archive, which is operated by the California Institute of Technology, under contract with the National Aeronautics and Space Administration under the Exoplanet Exploration Program. This research has made use of the Exoplanet Orbit Database and the Exoplanet Data Explorer at exoplanets.org. The authors would like to thank Thayne Currie for his useful (and rapid turnaround) comments on the manuscript.

Table 1. Model Best Fit Parameter Values[a]

Model	Confirmed	All KOI	KOI $> 5R_\oplus$	KOI $> 11R_\oplus$
Magnetospheric Truncation	$B_0 = 1.15$ kG, $\sigma = 0.17$	$B_0 = 2.90$ kG, $\sigma = 0.27$	$B_0 = 1.60$ kG, $\sigma = 0.22$	$B_0 = 1.20$ kG, $\sigma = 0.19$
Stellar Mass Independent	$log(A) = -1.35$, $\sigma = 0.17$	$log(A) = -1.10$, $\sigma = 0.28$	$log(A) = -1.25$, $\sigma = 0.23$	$log(A) = -1.30$, $\sigma = 0.20$
Dust Sublimation	$\sigma = 1.42$	$\sigma = 8.34$	$\sigma = 2.55$	$\sigma = 1.13$
Tidal Excitation	$\sigma = 3.70$	$\sigma = 12.46$	$\sigma = 4.50$	$\sigma = 2.25$
Uniform Random	...	...	...	...

[a]σ values are the Gaussian kernel widths in units of log(AU) that are convolved with the analytic 1:1 curves to produce the model density functions as described in §3. The units of $\log(A)$ are also log(AU).

Table 2. Relative Bayesian Posterior Probabilities (Unnormalized)[a]

Model	Confirmed	All KOI	KOI $> 5R_\oplus$	KOI $> 11R_\oplus$
Magnetospheric Truncation	1.618×10^{10}	2.444×10^{142}	2.702×10^{34}	9.597×10^{10}
Stellar Mass Independent	5.463×10^{8}	1.413×10^{141}	9.429×10^{33}	5.426×10^{10}
Dust Sublimation	1.699×10^{-15}	2.278×10^{27}	2.574×10^{16}	5.932×10^{4}
Tidal Excitation	1.540×10^{-15}	2.278×10^{27}	2.540×10^{16}	5.655×10^{4}
Uniform Random	1.176×10^{-38}	4.281×10^{-196}	1.204×10^{-35}	1.819×10^{-12}

[a]See Equation 10 and §4.1. These relative posterior probabilities include an overall normalization factor for each empirical data set to avoid the double data type machine precision limit. Consequently, we end up with probabilities greater than 1. The values to read from this table are the relative probabilities between models within a given data set, e.g. according to this analysis the magnetospheric disk truncation model for migration halting is $(1.618 \times 10^{10})/(5.463 \times 10^{8}) \sim 30$ times more favorable than the stellar mass independent model for the confirmed exoplanet data set.

Table 3. Reduced χ^2 Values

Model	Confirmed	All KOI	KOI $> 5R_\oplus$	KOI $> 11R_\oplus$
Magnetospheric Truncation	1.007	1.753	0.803	0.289
Stellar Mass Independent	3.227	2.308	0.908	0.386
Dust Sublimation	4.368	16.10	2.697	0.978
Tidal Excitation	4.391	16.09	2.699	0.985
Uniform Random	4.355	16.06	2.668	0.958

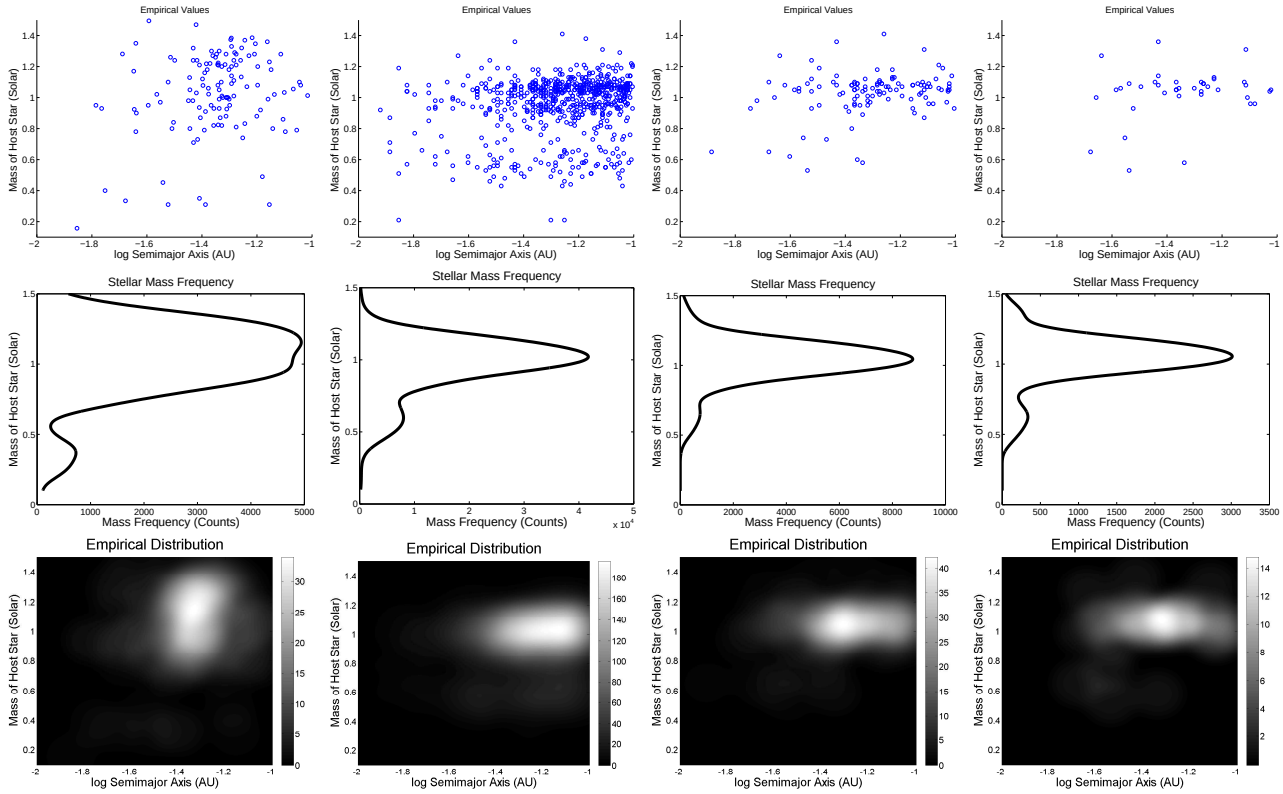

Fig. 1.— First row: Empirical distributions of exoplanet semi-major axes and host star masses for (from left to right): all confirmed exoplanets as of May 2011 (NASA Exoplanet Archive), all Kepler planetary candidates (Borucki et al 2011), all Kepler Planetary candidates with $R_{pl} > 5R_{\oplus}$, and all Kepler Planetary candidates with $R_{pl} > 11R_{\oplus}$. Second row: Planet frequency as a function of stellar mass for each data set in the first row, shown with arbitrary normalization. This is used as a normalization for our migration braking models to remove survey sample selection effects as a function of stellar mass. Third row: Empirical density functions generated for each data set using a method analogous to that in (Wasserman 2005).

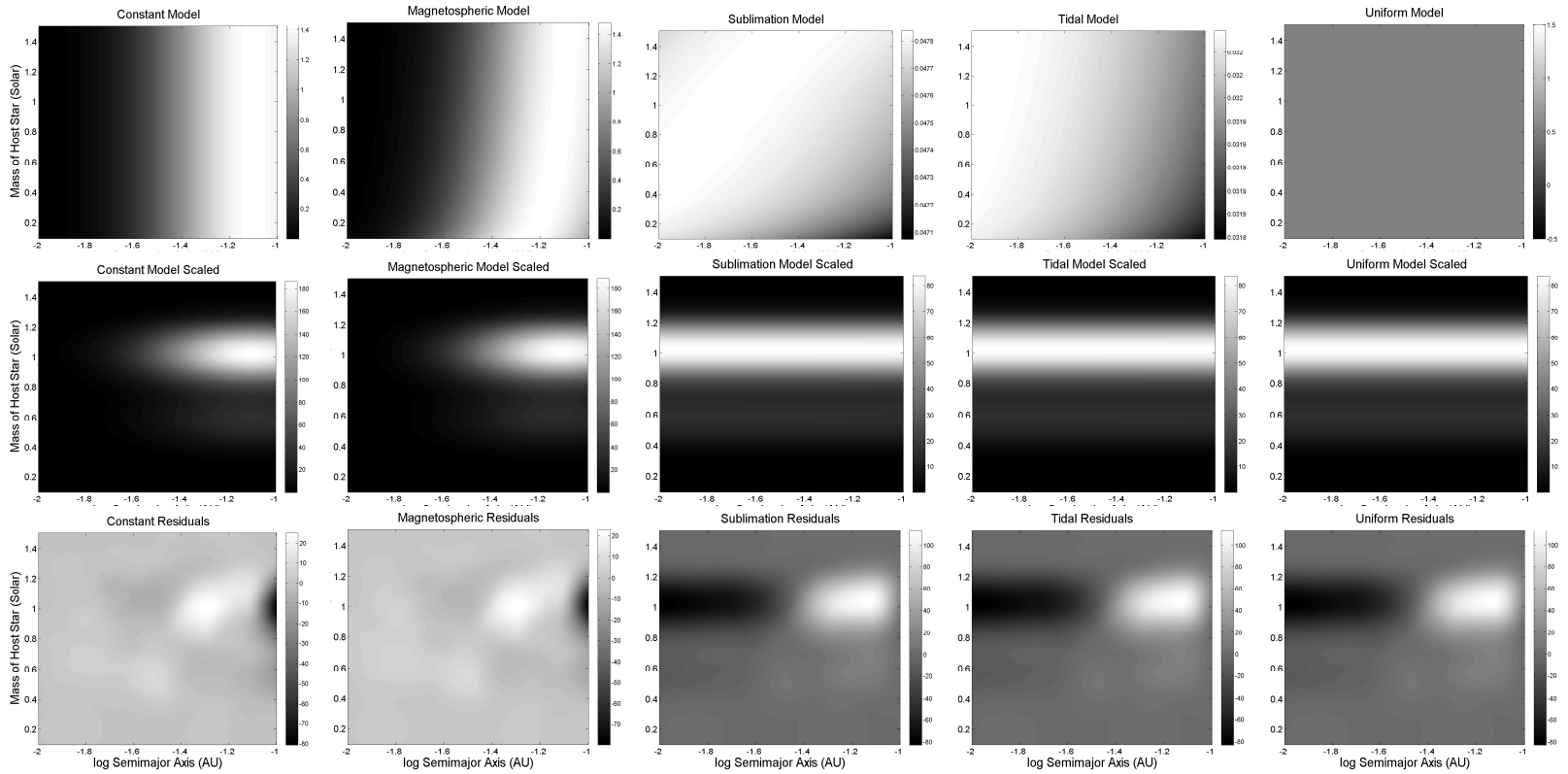

Fig. 2.— Sample: All Kepler planetary candidates. First row: Density maps for the best fits of the different migration braking models. Models are, from left to right: a fixed migration braking radius as a function of stellar mass; the interior 1:2 orbital resonance with the magnetospheric disk truncation radius; the interior 1:2 orbital resonance with the dust disk sublimation radius; tidal excitation of the convective atmosphere of the host star near the tidal disruption radius; and a uniform random distribution. Second row: The density functions from the first row scaled by the empirical planet frequency as a function of stellar mass. Third row: Residuals from the subtraction of the scaled model density functions from the empirical density function.

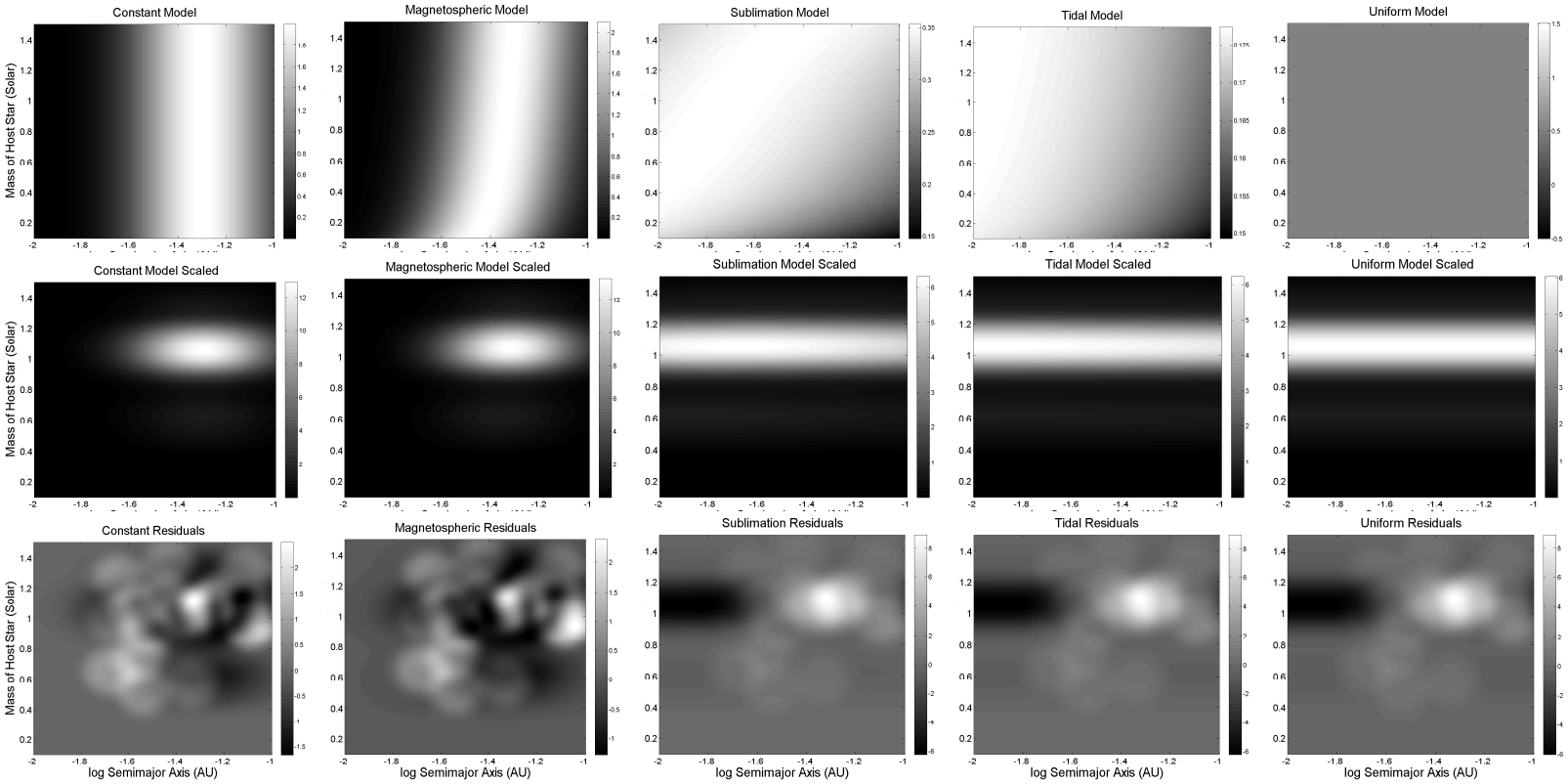

Fig. 3.— Same as Figure 2, except for the empirical sample: Kepler planetary candidates with $R_{pl} > 11R_{\oplus}$.

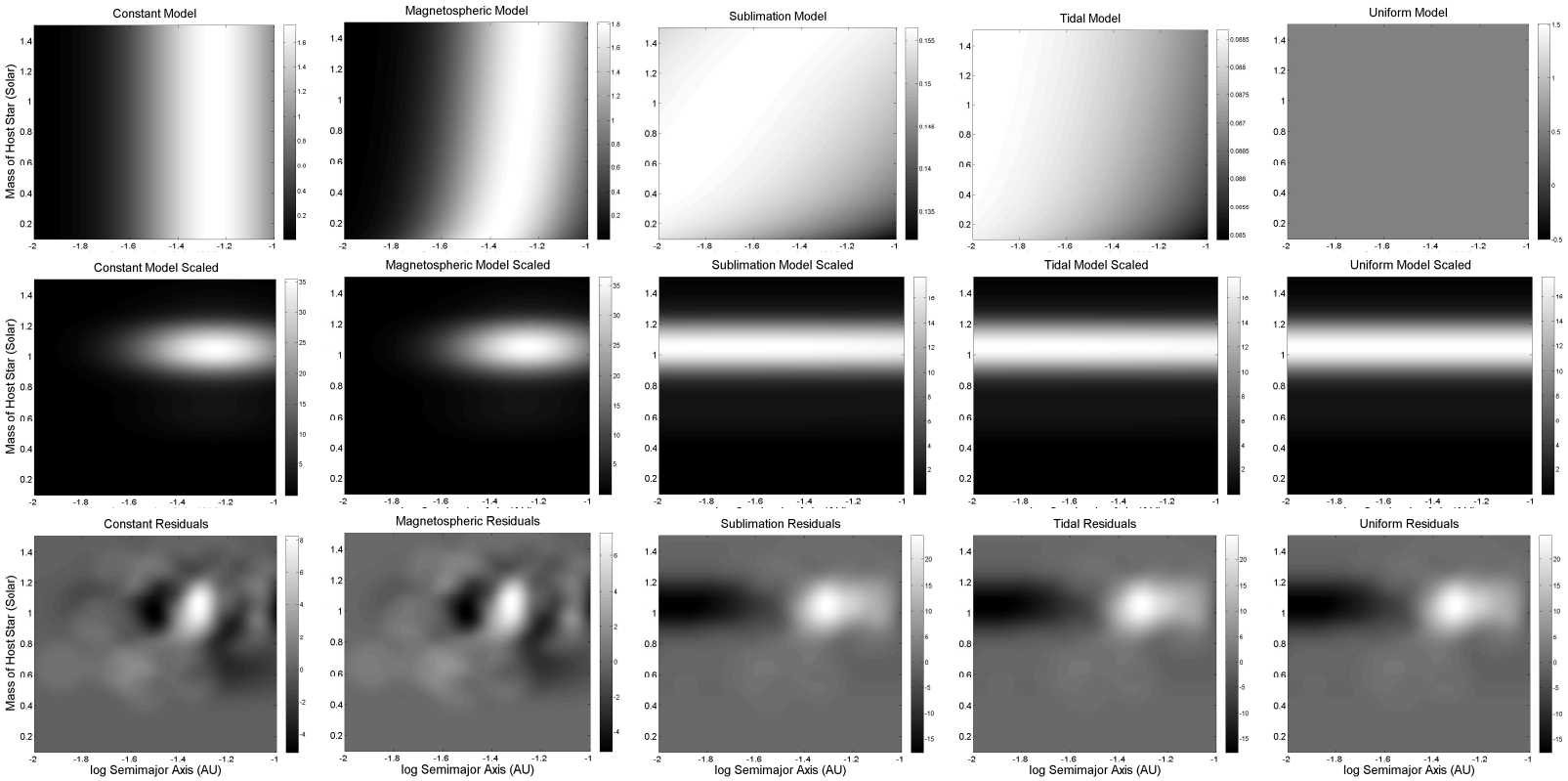

Fig. 4.— Same as Figure 2, except for the empirical sample: Kepler planetary candidates with $R_{pl} > 5R_{\oplus}$.

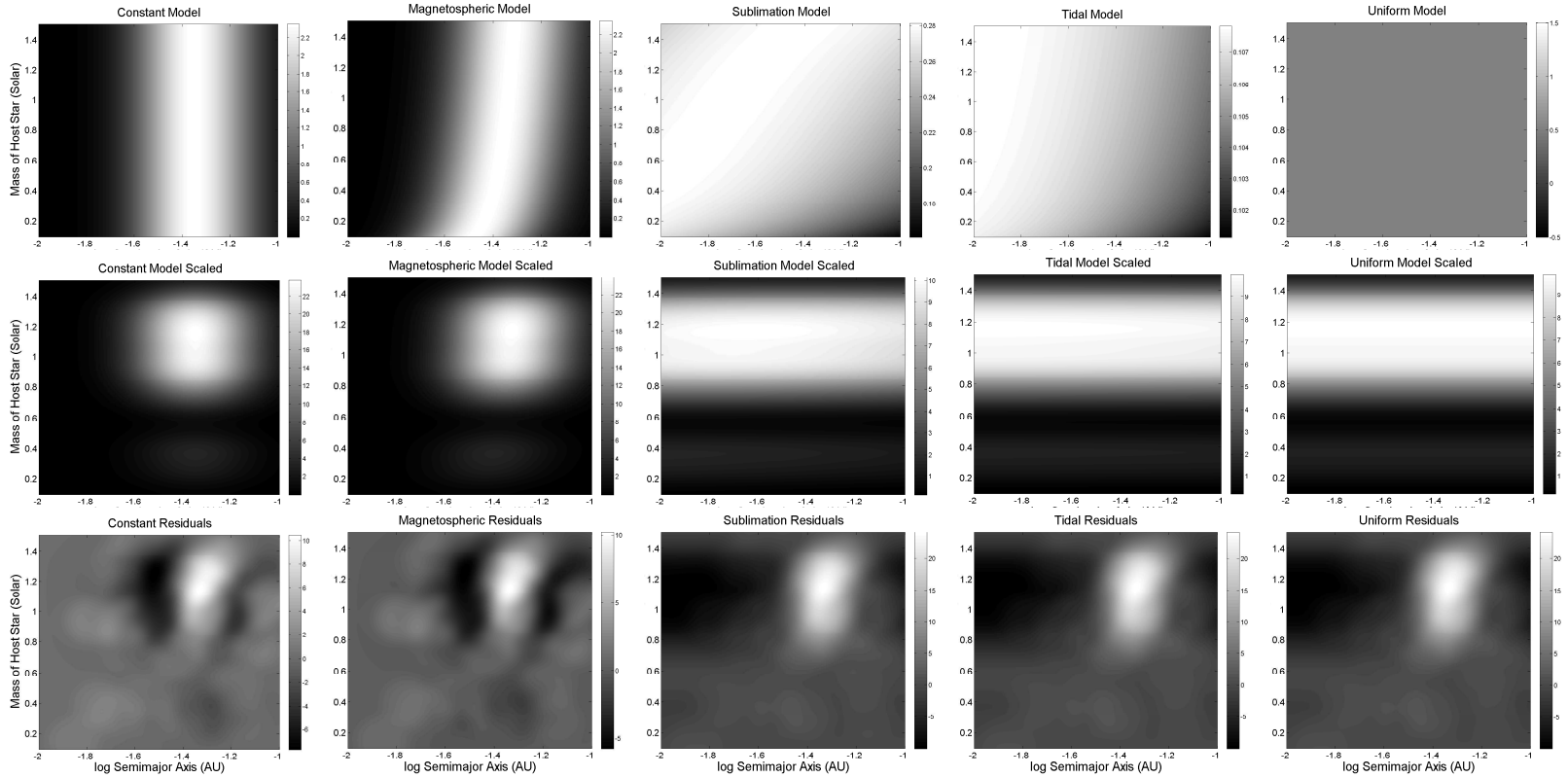

Fig. 5.— Same as Figure 2, except for the empirical sample: All confirmed exoplanets as of May 2011 (NASA Exoplanet Archive).

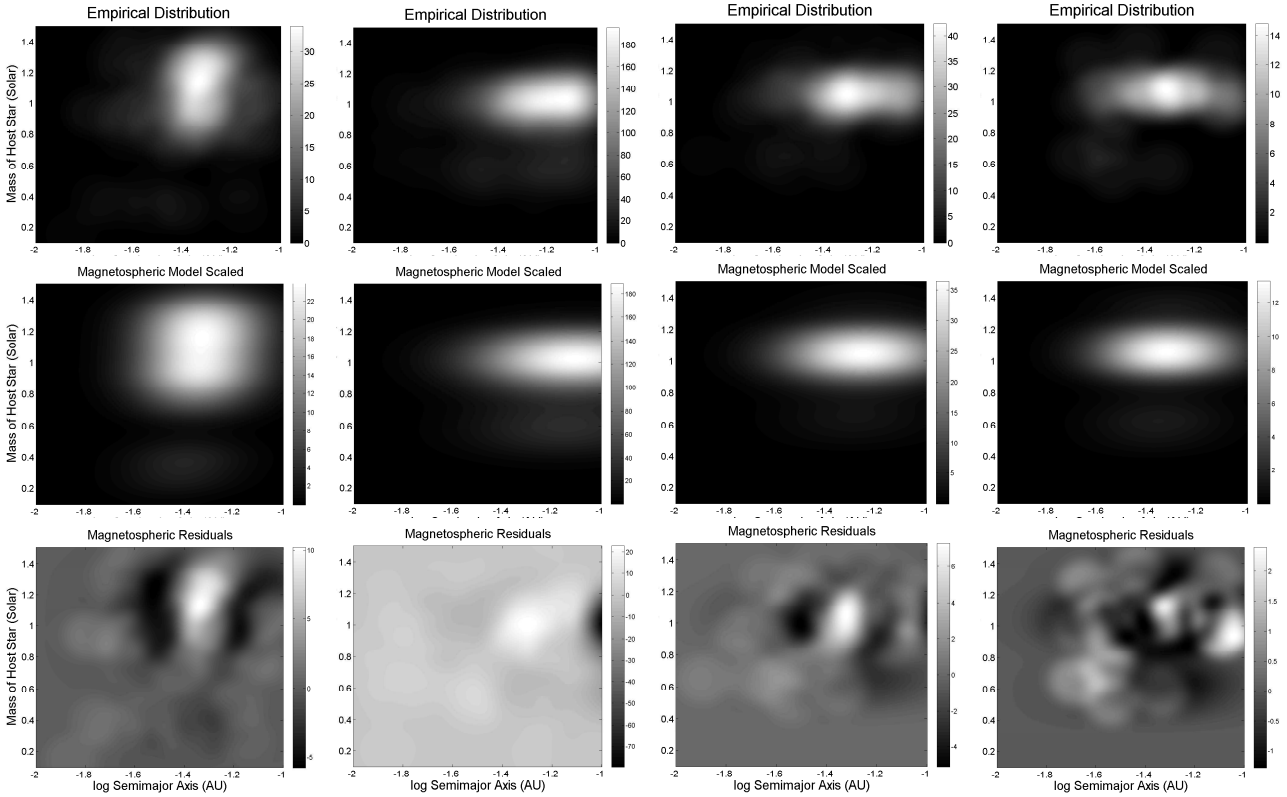

Fig. 6.— First row: Empirical density maps of (from left to right): all confirmed exoplanets as of May 2011 (NASA Exoplanet Archive), all Kepler planetary candidates (Borucki et al 2011), all Kepler Planetary candidates with $R_{pl} > 5R_{\oplus}$, and all Kepler Planetary candidates with $R_{pl} > 11R_{\oplus}$. Second row: For each of the data sets in the first row, the best fit model for migration braking via the 1:2 interior resonance with magnetospheric disk truncation radius. This model provides the best fit amongst all models tested for each empirical data set. Third row: The residuals from the subtraction of the scaled best fit density model from the empirical density map.

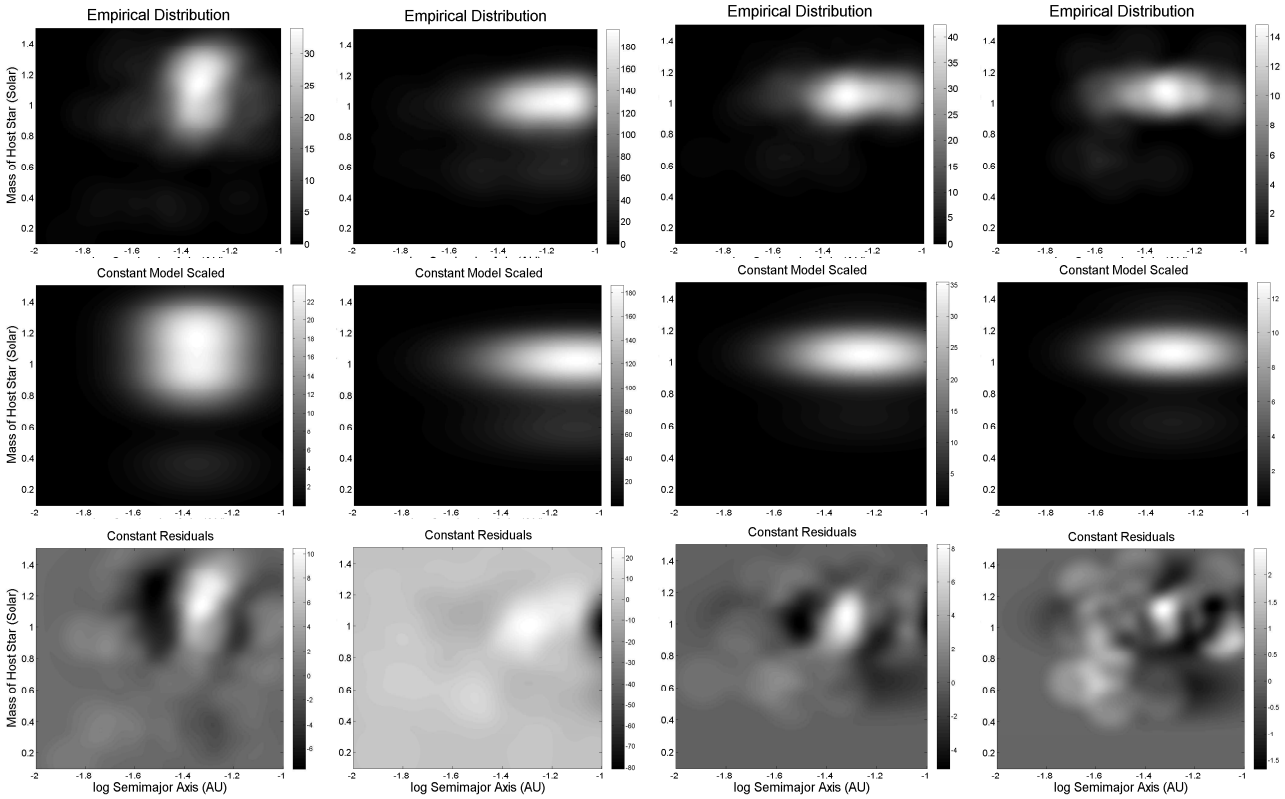

Fig. 7.— Same as Figure 6 for the model with migration braking at a stellar mass independent fixed semi-major axis.

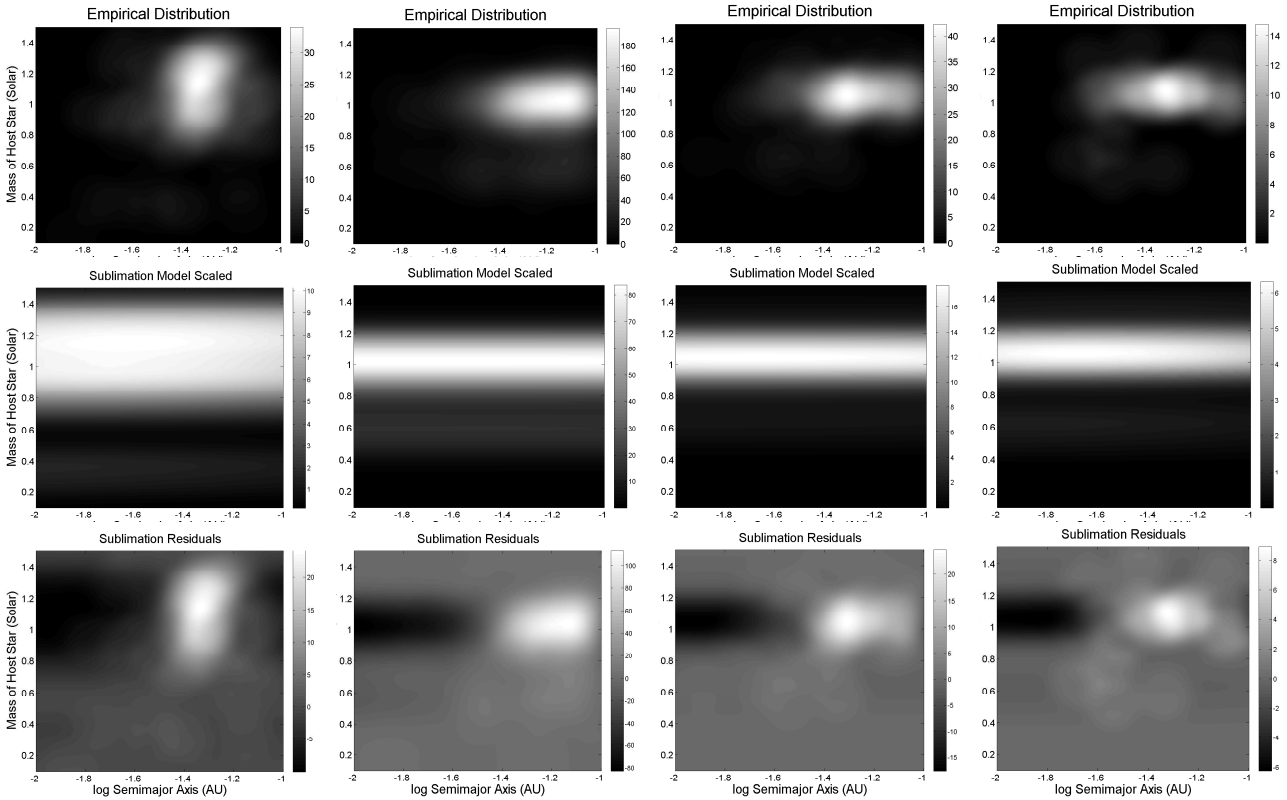

Fig. 8.— Same as Figure 6 for the model with migration braking model at the 1:2 interior orbital resonance with the dust sublimation radius.

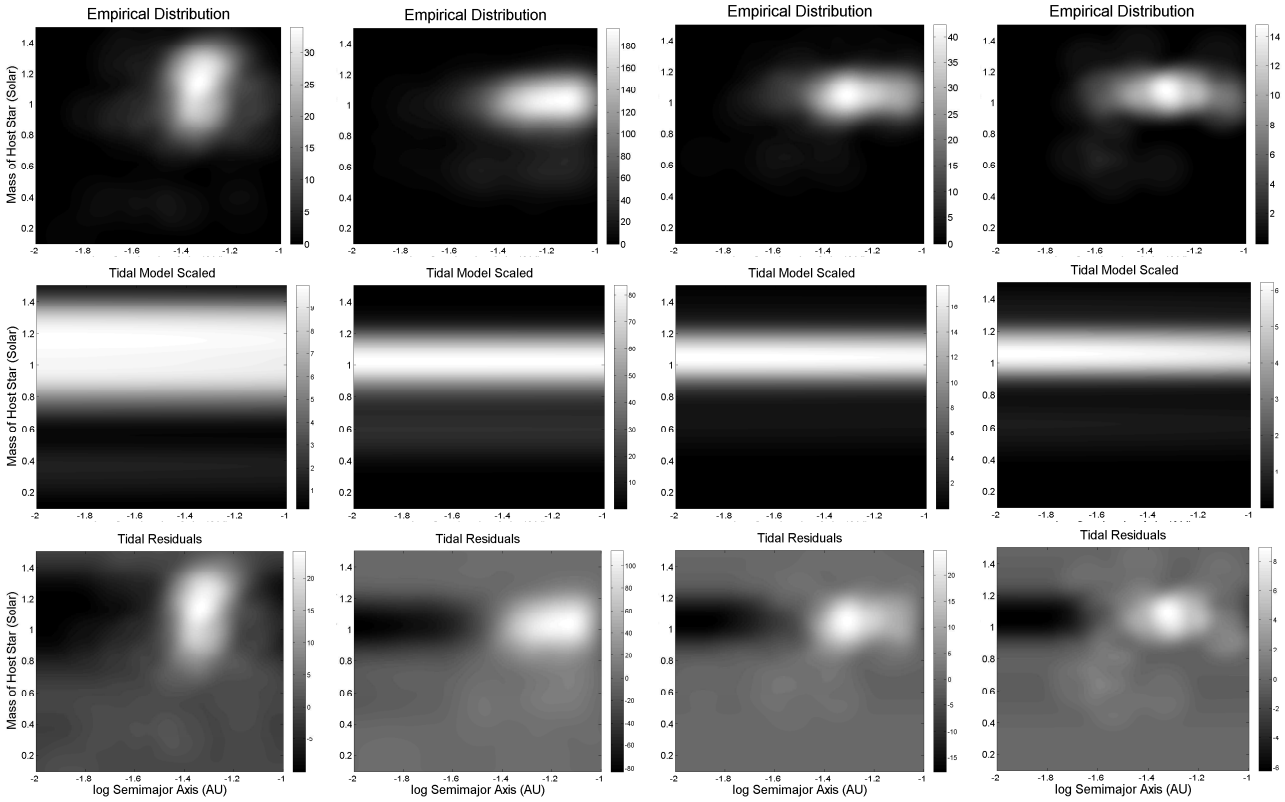

Fig. 9.— Same as Figure 6 for the model with migration braking from the tidal excitation of the convective atmosphere of the host star near the tidal disruption radius.

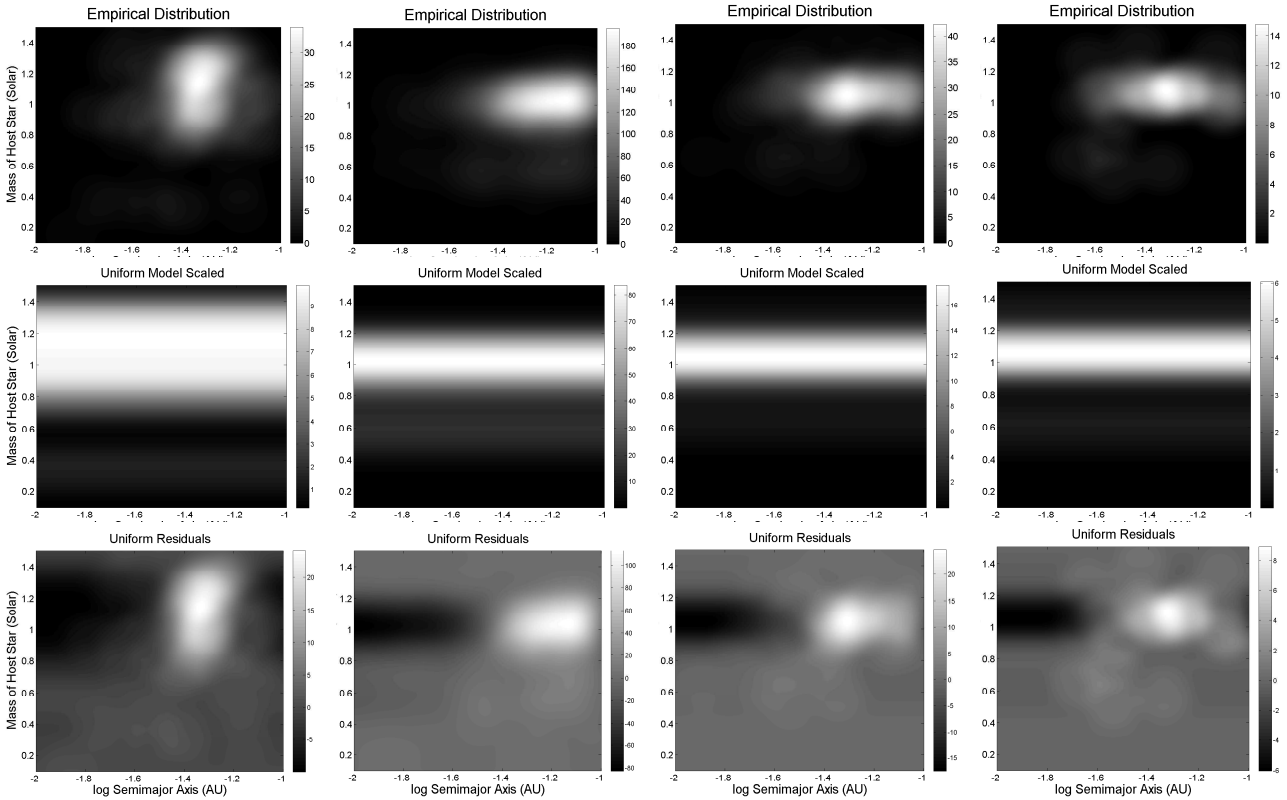

Fig. 10.— Same as Figure 6 for the model with migration braking at a uniform random location in the log of the semi-major axis.

REFERENCES

Arras, P., Burkart, J., Quataert, E., & Weinberg, N., 2011, MNRAS, submitted, arXiv 1107.6005

Baraffe, I., Chabrier, G., Allard, F., & Hauschildt, P., 1998, A&A, 337, 403

Bonls, X., et al., 2005, A&A, 443, L15

Borucki, W., et al. 2011, ApJ, 736, 19

Borucki,W., et al. 2010, Science, 327, 977

Brown, T., et al., 2011, AJ, 142, 112

Butler, P. et al., 2004,ApJ, 617, 580

Chiang, E. I., & Goldreich, P., 1997, ApJ, 490, 368

Currie, T. C., et a;., 2009, ApJ, 698, 1

D'Alessio, P., et al., 2006, ApJ, 638, 314

Eisner, J., et al., 2005, ApJ, 623, 952

Endl, M. et al., 2006, ApJ, 649, 436

Greene, T., & Lada, C., 1996, AJ, 112, 2184

Howard, A., et al., 2011, ApJ, submitted, arXiv 1103.2541

Johns-Krull, C. M., Valenti, J. A., & Gaord, A. D. 2003, Rev. Mex. AA Ser. Conf., 18, 38

Johnson, J.A., et al., 2011, ApJS, 197, 26

Jura, M., et al., 1998, ApJ, 505, 897

Kaib, N., Raymond, S., & Duncan, M., 2011, ApJL, 742, 24

Konigl, A. 1991, ApJ, 370, L39

Kozai, Y. 1962, AJ, 67, 591

Kuchner, M. J., & Lecar, M. 2002, ApJ, 574, L87

Lai, Dong, 2011,arXiv, 1109.4703

Lin, D. N. C., Bodenheimer, P., & Richardson, D. C. 1996, Nature, 380, 606

Lubow, S. H., & Ida, S., 2010, "Exoplanets," edited by S. Seager. Tucson, AZ: University of Arizona Press, 2010, p.347-371

Marcy, G., et al., 1997, ApJ, 481, 926

Marcy, G., & Butler, P., 1998, ARA&A, 36, 57

Matsumura, S., Peale, S., & Rasio, F., 2010, ApJ, 725, 1995

Menou, K., & Goodman, J., 2004, ApJ, 606, 520

Meyer, M., Calvet, N., & Hillenbrand, L., 1997,AJ, 114, 288

Morton, T., & Johnson, J., 2011, ApJ, 729, 138

Muzerolle, J., et al., 2003, ApJ, 592, 266

Nagasawa, M., & Ida, S., 2011, ApJ, 742, 72

Naoz, S., et al., 2011, Nature, 473, 187

NASA Exoplanet Archive, http://exoplanetarchive.ipac.caltech.edu

Plavchan, P., Jura, M., Kirkpatrick, J. D., Curti, R. M., & Gallagher, S. C. 2008, ApJS, 175, 191

Raymond, S., Mandell, A., & Sigurdsson, S., 2006, Science, 313, 1413

Rivera, E., et al., 2005, ApJ, 634, 625

Robitaille, T.P., et al., 2006, ApJS, 167, 256

Robitaille, T.P., et al., 2007, ApJS, 169, 328

Siess, L., Dufour, E., & Forestini, M. 2000, A&A, 358, 593

Silverstone. M., et al., 2006, ApJ, 639, 1138

Tanaka, H., Takeuchi, T., & Ward, W., 2002, ApJ, 565, 1257

Terquem, C., 2003, MNRAS, 341, 1157

Thies, I., et al., 2011, MNRAS, 417, 1817

Triaud, A.H.M.J., et al., 2010, A&A, 524 ,25

Tsang, D., 2011, ApJ, 741, 109

Watson, C.A., et al., 2011, MNRAS, 413, L71

Wasserman, L., "All of Non-Parameteric Statistics" , 2005, Springer, §6.3, ISBN-10: 0387251456

Wright, J.T., et al., PASP, 123, 412

Wu, Y., & Lithwick, Y., 2011, ApJ, 735, 109

Wu, Y., & Murray, N., 2003, ApJ, 589, 605

This preprint was prepared with the AAS LaTeX macros v5.2.